Invited Article: High-quality blazed gratings through synergy between e-beam lithography and robust characterization techniques

Cite as: Rev. Sci. Instrum. 96, 121303 (2025); doi: 10.1063/5.0293947
Submitted: 31 July 2025 • Accepted: 18 November 2025 •
Published Online: 5 December 2025

View Online

Export Citation

CrossMark

Analía F. Herrero,[1,2,a] Nazanin Samadi,[3,4] Andrey Sokolov,[1] Grzegorz Gwalt,[1] Stefan Rehbein,[1] Anke Teichert,[5] Bas Ketelaars,[6] Christiaan Zonnevylle,[6] Thomas Krist,[5] Christian David,[3] and Frank Siewert[1]

AFFILIATIONS

[1] Helmholtz-Zentrum Berlin, Albert-Einstein Str. 15, 12489 Berlin, Germany
[2] Physikalisch-Technische Bundesanstalt, Abbestr. 2-12, 10587 Berlin, Germany
[3] Paul Scherrer Institut, Center for Photon Science, Forschungsstrasse 111, 5232 Villingen PSI, Switzerland
[4] Deutsches Elektronen-Synchrotron DESY, Notkestr. 85, 22607 Hamburg, Germany
[5] NOB–Nano Optics Berlin, Krumme Strasse 64, 10625 Berlin, Germany
[6] RAITH B.V., De Dintel 27-A, 5684PS Best, The Netherlands

Note: This paper is part of the Special Topic on The 8th International Workshop on X-Ray Optics and Metrology.
[a] **Author to whom Correspondence should be addressed:** analia.fernandez.herrero@ptb.de

ABSTRACT

Maintaining the highest quality and output of photon science in the VUV-, EUV-, soft-, and tender-x-ray energy ranges requires high-quality blazed profile gratings. Currently, their availability is critical due to technological challenges and limited manufacturing resources. In this work, we show the developed method for manufacturing blazed gratings relevant for synchrotron-based science by means of electron-beam lithography (EBL). We investigate different parameters influencing the optical performance of blazed profile gratings and develop a robust process for the manufacturing of high-quality blazed gratings using polymethyl methacrylate as a high resolution positive tone resist and ion beam etching. Finally, we demonstrate excellent agreement in efficiency between the produced EBL grating and the theoretical prediction.

© 2025 Author(s). All article content, except where otherwise noted, is licensed under a Creative Commons Attribution (CC BY) license (https://creativecommons.org/licenses/by/4.0/). https://doi.org/10.1063/5.0293947

08 December 2025 09:12:47

I. INTRODUCTION

The EUV, VUV, and soft x-ray energy regions are of great interest to industry and academia alike. For instance, the so-called water window, essential in natural sciences, is located within these regions. The EUV region, in turn, has seen great development in materials science and coatings for the semiconductor industry and astrophysics during the last decades. Accelerator-based photon sources have seen an enormous improvement in terms of brilliance, stability, and coherence.[1] Not only large-scale facilities but also lab sources have increased their stability and power in the EUV and soft x-ray energy ranges. For photonic sciences to capitalize on these advances, the availability of high-quality blazed gratings is essential.[2–4] Blazed gratings show substantially higher diffraction efficiency than their laminar counterparts. They are used in monochromators in broadband emission sources as well as analyzers in spectroscopical applications in these energy regions. In the case of applications at free electron lasers, blazed gratings are of interest, as they show a higher damage threshold compared to lamellar gratings.[5,6] Furthermore, it has been shown how the tender x-ray region can also benefit from the availability of high-quality blazed gratings coated with a dedicated multilayer.[7–9] Working at photon energies between 1.5 and 3 keV usually requires operating crystal monochromators near to normal incidence, which causes thermal instabilities and limits their

usability. However, using multilayer coated blazed gratings, efficiencies up to 60% can be achieved.[7] In this regard, the significance of the antiblaze-to-blaze ratio for the optimal performance of blazed profile gratings has been highlighted in the literature.[10] Therefore, to ensure the highest quality of beamline and end-station performance at photon sources from the VUV to the tender x-ray region, it is essential to explore new and more versatile fabrication methods for such gratings that can meet their specific requirements.

Mechanical ruling of blazed gratings is a common and established technique.[11,12] However, it is time consuming, poses high technological risk, and is offered in only a very few places around the world. Moreover, the method is less versatile than others that can locally adapt the profile to counteract any feature of the structure or substrate. During the last decades, other methods have been investigated. Reasonable results have been obtained for low line densities and very shallow angles by nanoimprinting.[13] However, high-resolution spectrometers require high line densities, which is challenging for most of the above-mentioned methods. In addition, high blaze angles at high line density gratings are a challenge in imprinting technology. The first tests on anisotropic etching through a mask or patterned area followed by anisotropic etching for the production of a blazed profile grating date back to the 1980s.[14,15] This method allows a very low facet roughness but might result in a plateau on the apex region of the grating that negatively impacts the grating efficiency. In addition, steps have been included to reduce the area of this region while maintaining the region's sharpness.[16–18] However, the control of the antiblaze-to-blaze angle cannot be achieved, and the efficiency is thus affected. Furthermore, this approach is limited to plane substrates while curved (spherical or cylindrical) substrates cannot be patterned with sufficient precision. Grey-tone electron-beam lithography (EBL) has also been explored in the last decades as an alternative method for the production of optical elements.[19,20] Tests for the manufacturing of blazed profile structures have been conducted using a dose variation of the EBL[21] as well as with frequency variation[22] of the e-beam writer exposure. In this method, the resist is exposed to a variable dose, and afterward, the patterned resist is transferred into the substrate, for instance, by ion beam etching[23] or oxidation[24] depending on the resist. As the slope of the facet can only be approximated by a certain number of steps, methods have been developed to reduce the waviness of the facet. For polymer-based resists, thermally activated selective topography equilibration (TASTE) has been previously reported in the literature as the most suitable method to reduce the roughness of the blazed facet.[22,25] Previous studies show very good results in the production of high line density blazed gratings for EUV and soft x-ray spectroscopy for astronomical applications.[26,27] However, thermal reflow may induce changes in the shape of the grating profile, such as changing the antiblaze-to-blaze ratio, which is essential in synchrotron optics. For this reason, an adapted exposure, where the apex region is unexposed, has been proposed.[28] No studies have been performed so far for relevant grating parameters in synchrotron optics in the soft x-ray energy range, i.e., low line densities and low blaze angles.[29] In the present study, higher efficiency output is pursued by optimizing the facet roughness as well as pattern fidelity.

Developing new methods, i.e., a sustainable fabrication process, requires metrology methods that can track these changes and give feedback on the process. EBL possesses all the requisites to produce a high-quality blazed-profile grating. It allows the patterning of large areas in a short time compared to the time consuming mechanical ruling, and it is much more flexible in terms of shape-patterning. However, to ultimately establish a reliable method for the fabrication of future smart gratings, a critical and systematic analysis of all the steps is needed.

We report the development of a method for fabricating blazed profile gratings with extremely low facet roughness, based on electron beam lithography (EBL) and supported by high-precision metrological process control. In this study, we focus on very shallow blaze angles (less than 1°) and moderate line densities. The limits of the adapted EBL exposure strategy in preserving a sharp apex region are investigated. A polymer-based resist, polymethyl methacrylate (PMMA), was used for patterning, and various temperatures and heating durations were tested during the thermal reflow step to determine the optimal conditions for producing high-quality blazed profiles. After transferring the patterned structures into silicon via ion beam etching, facet roughness values close to the nominal surface roughness of the silicon wafer were achieved. The structures were characterized using atomic force microscopy (AFM) and at-wavelength metrology to validate the fabrication process and establish the reliability of the technology.

II. METHOD

For the development of the lithography method, a moderate line density of 600 lines/mm was chosen. Blazed gratings of that line density can be found in monochromators and analyzers in the soft x-ray energy range, e.g., at the BESSY-II synchrotron.[30–32] In addition, the development of the lithography process emphasized establishing a highly reproducible and stable technology line for patterning blazed-profile structures into silicon. The latter would be an essential advantage compared to the classical mechanical ruling, where every second to third approach of ruling failed.

For the optimization of the process, it is inevitable to develop a systematic approach for controlling the different steps. Figure 4(a) shows a straightforward method for obtaining the nano-patterning of a grating processed into a substrate of single crystal silicon using EBL. Additional steps, Figs. 4(b) and 4(c), were introduced to this approach to further reduce the facet roughness or have better control of the apex region of the blazed profile grating. The e-beam writing process has been carried out at Helmholtz-Zentrum Berlin (HZB), as well as the *ex-situ* and at-wavelengths characterization. The transfer of the e-beam written pattern from resist into the wafer was performed by means of Ar^+ ion beam etching at NOB Nano Optics Berlin GmbH (NOB).

A. Manufacturing

The process has been developed on 4-in.-Si wafers (100), under the consideration that it will be transferred to a thicker substrate (up to 10 mm) in a future stage. Si-wafers are spin-coated with PMMA (671.02, *Allresist GmbH*) at 2500 rpm. Higher spin-coating speeds, if possible, were avoided because, for a thick, heavy, rectangular shaped substrate, the spin-coater speed is limited. After spin-coating, the wafers are baked in a convection oven at 180 °C. Unlike the more commonly used hotplate method, the convection

08 December 2025 09:12:47

© Author(s) 2025

oven helps minimize the influence of varying ambient conditions, such as temperature or humidity, on a final structure.

1. Electron beam lithography

The e-beam system used for patterning is an EBPG5000 Plus from RAITH. EBL exposure parameters of 100 kV acceleration voltage and 10 nA beam current were used. For the production of blazed profile gratings, different techniques for the electron beam exposure can be used. One method consists of tuning the dose per shot along the grating period, following the decay that corresponds to the blaze angle. Another method is multipass writing, which consists of varying the shots per area, increasing or decreasing the dose density, and reaching a similar effect. Moreover, a combination of the two approaches is also possible, obtaining smoother transitions on the blazed profile at the cost of the exposure time.

Here, for the sake of simplicity, we have divided the blaze angle into sections and adapted the doses along the blaze facet of the grating to obtain a gradient on PMMA that is then transferred to the Si-wafer by means of ion beam etching. The blazed facet is approximated by a finite number of steps, and the dose is changed accordingly to obtain the desired slope. Figure 1 shows the contrast curve after the exposure. This curve allows us to select the dose variation according to the blaze angle to be obtained, accounting for the selectivity rate of Si to PMMA according to Fig. 3. We used a custom Python script to generate the GTX file, which allow us to select random periods and blaze angles by varying the dose range. If the periods are not a natural multiple of the beam step size, the patterns are scaled for the exposure. This file is subsequently converted into the Raith EBPG pattern data format (GPF).

The exposure areas for the test fields are $20 \times 5\ \text{mm}^2$. The field produced following the developed recipe and shown in Fig. 8 has dimensions of $80 \times 5\ \text{mm}^2$.

2. Development

After exposure, the samples are dipped in a bath of methyl isobutyl ketone (MIBK; ALLRESIST, AR 600-56) for 60 s and then in a stopper (AR 600-60, ALLRESIST) for 10 s. After this process, the blazed profile structures on PMMA are on the wafer. As previously reported,[33] the contrast curve of PMMA is sensitive to the delay between exposure and development. In this context, such variations would result in deviations in the resulting blaze angles. Through iterative processing, we identified inconsistencies potentially related to the time delay between exposure and development, also affecting the roughness and homogeneity. Therefore, a limited test study was performed, where samples were developed at different times after exposure. In our test, it was observed that macroscopically the overall homogeneity of the fields was affected; then the samples were measured using AFM at the center and closer to the edges of the field, analyzing the facet roughness. The dependency on the time span between exposure and development is shown in Table I. The test was performed using six different fields on the same wafer, and after the exposure, the wafer was taken out of the system and kept in ambient conditions in a clean room. The roughness value corresponds to the standard deviation over all measured points within the field. In addition, for the analysis, any deviation from a perfect facet line is considered. The values for the blaze angle and height correspond to the average and standard deviation of all analyzed data for each field. Therefore, the non-uniformity of the blazed profile grating can be seen in the standard deviation of the height. It should be noted that the absolute values of the roughness and the waiting times are not statistically significant, and these will also depend on ambient conditions. Follow-up work might help to better analyze other factors that are influencing these results.

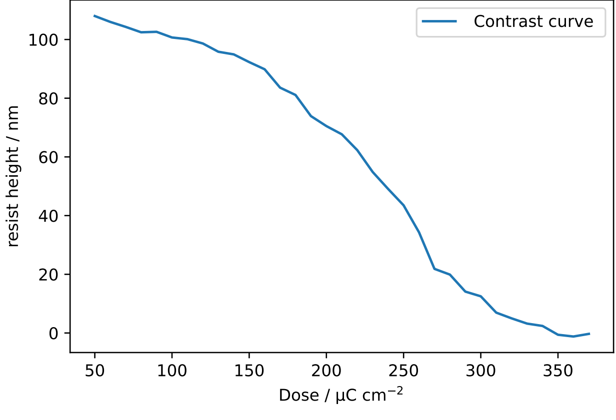

FIG. 1. Contrast curve obtained on PMMA.

TABLE I. Facet roughness on PMMA measured with AFM depending on the waiting time between exposure and development. Please notice that the difference between the blaze angles for similar heights is due to different antiblaze angles.

Waiting time (h)	Blaze angle (°)	Height (nm)	Roughness (nm)
$6 < t < 12$	1.51 ± 0.08	37.5 ± 1.6	1.8
$14 < t < 24$	1.43 ± 0.08	31.6 ± 0.6	1.6
>72	1.23 ± 0.06	31.5 ± 0.5	1.4

3. Tempering

Thermal annealing of 3D polymer-based structures has already been tested in the literature.[25] However, the studies did not include large periods of grating with very shallow blaze angles and over large structured areas. By thermally annealing the blazed PMMA gratings, the facet roughness is reduced. The samples were annealed using a convection oven, allowing for a uniform distribution of the hot air. The gratings were loaded, and the temperature was ramped up to enable thermal reflow. They were held at the target temperature for a defined period. Both the reflow temperature and the annealing time were parameters under investigation (see Table II).

However, thermal reflow can also impact the shape of the apex region of the grating. This step is critical for the production of high-quality blazed gratings with a good antiblaze-to-blaze ratio and low facet roughness. Figure 2 shows the dependency of the grating efficiency on the antiblaze-to-blaze ratio. The calculation was performed for the soft x-ray energy region using REFLEC and considering 600 lines/mm gratings in Si, a blaze angle of 0.7°, coated with 30 nm gold, in non-conical mounting, and with a grazing angle of incidence of 4°. The distribution changes depending on the angle of incidence, and it will shift the maxima in the energy axis depending on the blaze angle of the grating. However, the results

08 December 2025 09:12:47

© Author(s) 2025

TABLE II. AFM analysis of 600 lines/mm gratings in PMMA before (rms_i) and after (rms_t) thermal treatment at various temperatures. The vertical line separates the roughness (rms_e) and antiblaze-to-blaze ratios obtained after etching. The standard deviation corresponds to the dispersion of the measured values for each grating.

Sample	rms_i (nm)	T (°C)	t (min)	rms_t (nm)	Antiblaze to blaze	rms_e	Antiblaze to blaze
0	1.5	...	...	...	12 ± 5	1.05	11 ± 5
1	1.5	105	120	1.3	9 ± 4	0.85	9 ± 5
2	1.6	115	120	0.7	6.0 ± 0.7	0.34	5.6 ± 0.8
3	1.5	120	120	0.4	3.8 ± 0.3	0.22	3.5 ± 0.6

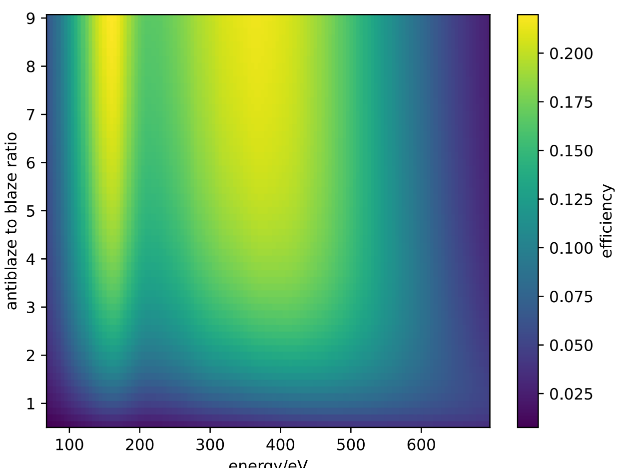

FIG. 2. Efficiency calculation using REFLEC for the first order of a silicon blazed grating with 600 lines/mm and coated with 30 nm gold in the depicted energy range. Having a larger antiblaze-to-blaze ratio ensures better grating performance.

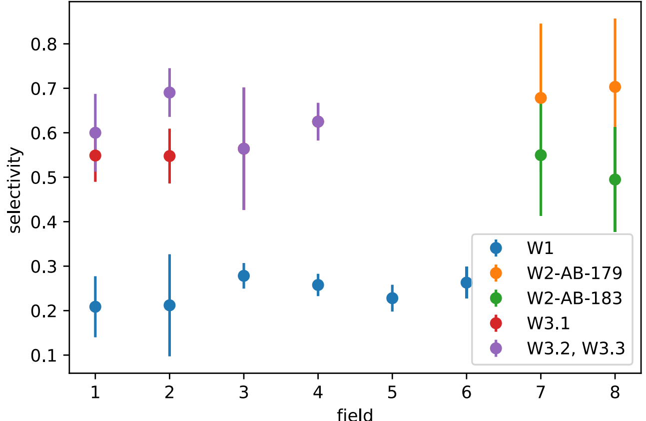

FIG. 3. Selectivity rates of Si/PMMA for different setups. The different colors correspond to different wafers and tests of the etching process.

show that, for a given incoming angle and blaze configuration, larger antiblaze angles are crucial for achieving high-quality grating performance. Consequently, the development focused on optimizing the antiblaze-to-blaze angular ratio.

4. Ion beam etching

The structure produced on PMMA is then transferred into Si by ion beam etching at NOB Nano Optics Berlin GmbH. The etching machine of NOB allows us to etch substrates with surfaces up to 200×200 mm^2 and a thickness up to 30 mm. Etching depths from a few nm to 100 nm are possible. The substrates are moved during the etching process, and different areas can be selected by an aperture above the sample, allowing different depths to be etched in one process. In addition, depth gradients in one direction can be reached. Due to the different etching rates of Si and PMMA, after etching, the angles and roughness will be smaller. Figure 3 shows the selectivity rates of Si/PMMA for different sampled sets. The final height of the structures and, consequently, the final blaze angle, depends on this step. Therefore, this selectivity must be taken into account for creating the exposure file. The values were calculated based on the measurement of the profiles with AFM before and after etching. The colors on the graph indicate the same wafer, which was produced with different grating fields. The dispersion in the measurements corresponds to variation within the fields, causing variation of the blaze angles. For this case, a 600 lines/mm grating and 0.75° blaze angle and 12 cycles at the speed of 0.57 mm/s were performed, obtaining a blaze angle variation smaller than 0.1°.

B. Metrology

Every step of the process was analyzed using appropriate measurement methods to establish a reproducible technique for patterning blazed-profile structures, highlighting the essential role of metrology. To this end, control of the various steps was performed using both *ex-situ* and at-wavelength tools, resulting in a systematic approach (see Fig. 4).

1. Ex-situ metrology

Scanning force microscopy, usually called atomic force microscopy (AFM), was used to measure the facet roughness as well as the blazed profile. The atomic force microscopy measurements were performed at HZB. AFM measurements were performed with a Nanosurf FlexAFM 100×100. The custom-made AFM from Nanosurf can host samples of up to 1 m in length and 100 mm in thickness. The grating was measured under dynamic mode conditions with a standard pyramidal shaped silicon probe (Tap 190 AL-G) with a nominal tip radius of <10 nm. The inspected area is 15×5 μm^2, with 4500 points in the longer axis and 500 lines for the short axis.

08 December 2025 09:12:47

© Author(s) 2025

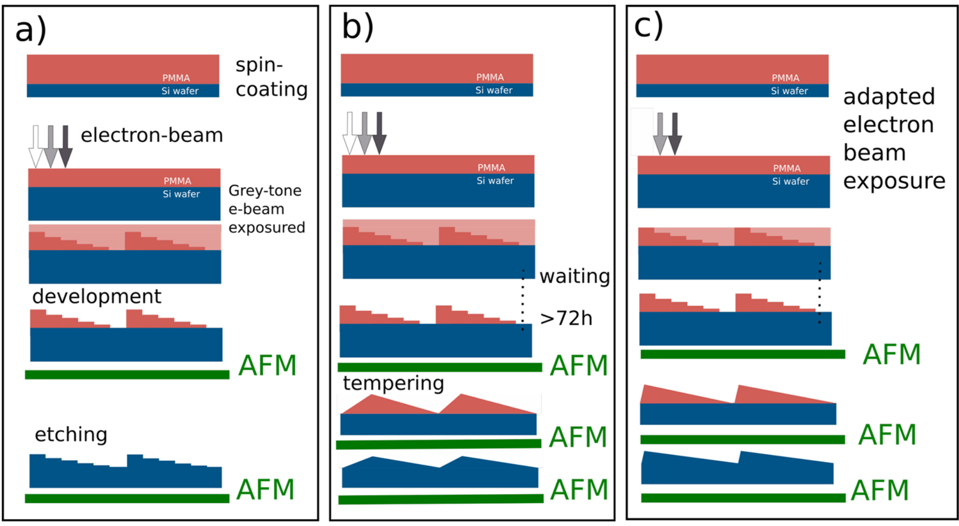

FIG. 4. Manufacturing processes and metrology methods used to control the processing of the gratings. (a) Shows the skeleton of the production of blazed profile gratings in a general way using EBL and PMMA as positive resist. In (b), tempering is included in the process to reduce the amount of roughness. At the end, see (c); in addition, waiting time between the exposure and developing was introduced as well as the adaptation of the writing process to better control the apex region of the gratings and counterbalance the effect of tempering. It should be noticed that by using the shape *gradient cube* for e-beam exposure, the transition between the EBL exposure doses is smoother.

These measurements allow us to verify the best strategy to follow or whether introducing further steps in the lithography process might be advisable. Systematically, several images were taken from the different fields and then analyzed using a Python routine, developed in-house, and based on the software Gwyddion.[34,35] The code was benchmarked with Gwyddion, obtaining very good results (1% deviation) for this type of grating and reducing the amount of processing time drastically. The presented values in this paper correspond to the extracted parameters and the standard deviation from all the measurements of the field.

2. At-wavelengths metrology

The at-wavelength metrology was performed at the Optics Beamline at BESSY II[31,36] during several measurement campaigns. This beamline is dedicated to accurate wavelength metrology on sophisticated XUV and soft x-ray optical elements like reflective or transmission diffraction gratings, multilayered systems, reflection zone plates, etc. The higher order suppression system of the beamline provides spectrally pure intensity in the photon energy range from 12.5 eV up to 1850 eV, which is useable for quantitative measurements of reflection, diffraction, or transmission. The UHV 11-axis reflectometer can handle both small test samples and real-size optics up to 550 mm in length and up to 4 kg. It has goniometers for 360° in-plane rotation for the sample and detector stages. The sample stage is supported by an UHV tripod, which provides *in situ* motion of six degrees of freedom for accurate alignment and mapping of the surface of the tested sample. Various apertures in front of the detectors allow recording of the full beam reflected or diffracted from the sample as well as resolution of scattered intensity in the plane of the incident beam. The beam size in the sample position of (0.35×0.25) mm^2, vertical × horizontal, provides an optimal spot size on the sample and a rather small vertical beam divergence of 0.5 mrad. The gratings were mounted in non-conical geometry, i.e., grating lines perpendicular to the incoming beam. In addition, they were characterized by the collection of scattered and diffracted signals in a plane to obtain their efficiency and uniformity, as well as their dispersion pattern. The incoming intensity was measured both before and after the measurements with the same diode to assess stability, and then it was used for normalizing the data.

Measurements of the dispersion curves were performed at a fixed photon energy of 400 eV and an incidence angle of 4°. The detector arm was rotated to capture the scattered signal from both the zero and first diffraction orders, as well as the diffuse scattering in between. For the efficiency measurements, the incidence angle remained at 4°, while the first-order diffraction signal was recorded across a range of photon energies. The beamline energy was scanned from 60 to 700 eV. The chosen incidence angle ensured that the small test fields were not over-illuminated while still providing a sufficiently strong signal for reliable statistics.

III. RESULTS AND DISCUSSION

A. Blazed profile fidelity

To fabricate the blaze-profile grating, elementary shape primitives such as *path* or *trapezoid* shapes in the EBPG were utilized and tested. With the *trapezoid*, the blazed facet is divided into rectangular terraces with increasing doses from the apex to the lower region of the blazed facet. To analyze the influence of the steps approximating the blazed profile, a set of samples was produced, considering 7, 17, and 119 (using *path*) dose steps by a beam step size (BSS) of 0.014 μm. By using the *path*, each step across the blaze has a different dose. According to the results, small variations to the blaze angle were observed (less than 5%) between the different approaches. The field whose facet is approximated by fewer steps presented shallower blaze angles. We attribute this effect to the large terraces used to approximate the facet gradient, together with the proximity effect, which leads to less pattern fidelity. The terraces are wider when the number of steps is smaller. The applied average doses are slightly

08 December 2025 09:12:47

© Author(s) 2025

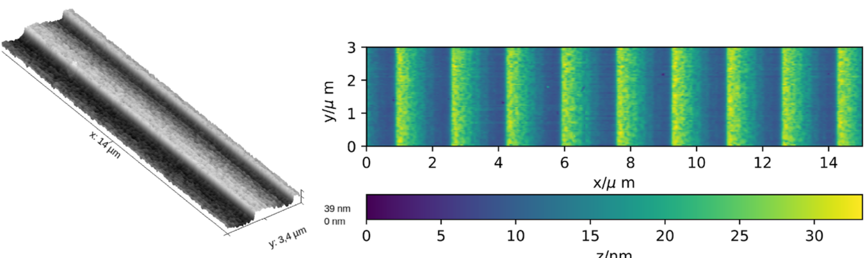

FIG. 5. Facet roughness up to 1.5 nm is obtained for the structures on resist (PMMA) before they are tempered or transferred into the substrate. In this case, the blazed profile was approximated by seven steps.

different and would result in a different resist height after development. If not indicated otherwise, the shown gratings correspond to blazed facets approximated by 17 steps. Using this number of steps and the process shown in Fig. 4(a), facet roughness as low as 1.5 nm was achieved on PMMA (see Fig. 5), going down to 1.09 nm after etching, still larger than nominal values for Si. Although increasing the number of steps reduced the facet roughness slightly, the improvement was not sufficient to eliminate the need for tempering.

B. Facet roughness and apex angle

A test was performed for different tempering temperatures during 120 min, which led to a great reduction in the roughness. However, the antiblaze-to-blaze ratio is also affected in this process, resulting in a slightly different shape. The results are listed in Table II. They show the correlation between the tempering temperature, the reduction of the roughness, and the antiblaze-to-blaze ratio, which might lead to a reduction of the efficiency of the grating.

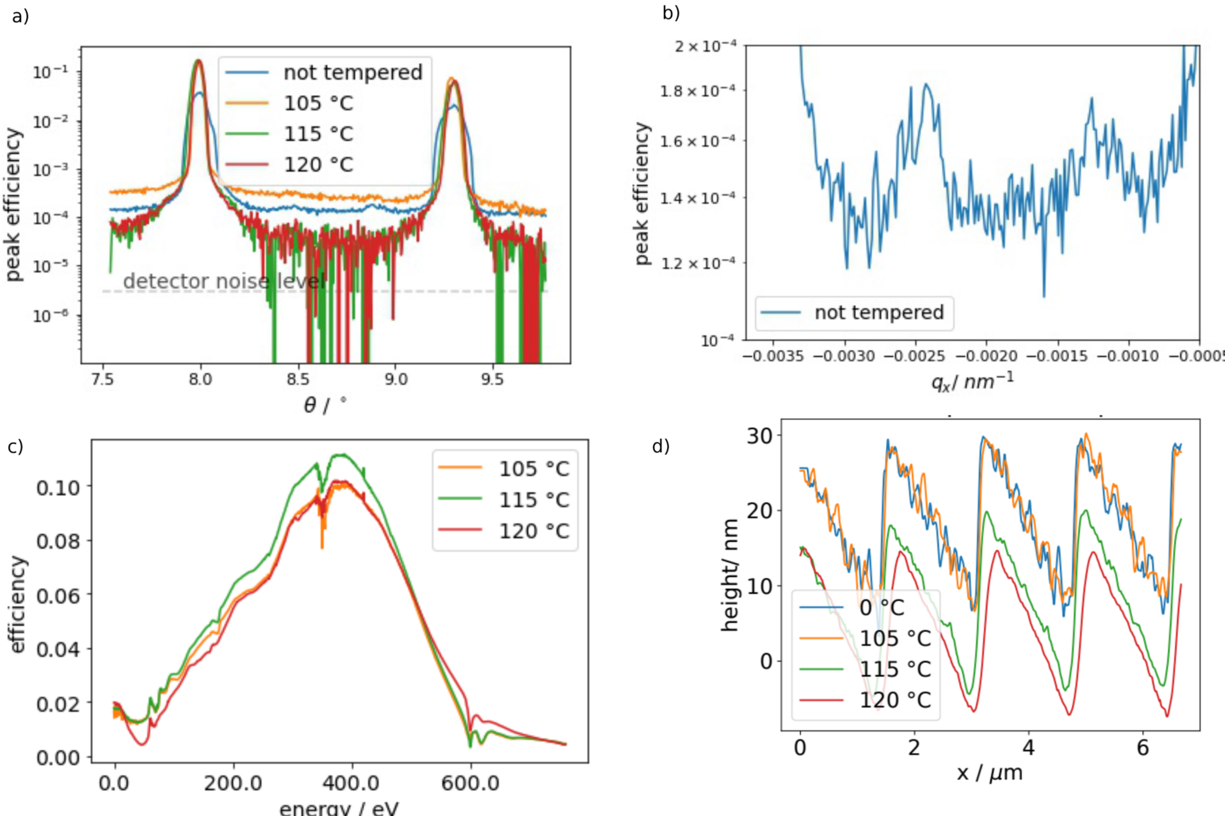

FIG. 6. (a) Dispersion curves of the etched gratings without being annealed (blue) and after tempering for three different temperatures during 120 min. The grating that was not tempered shows the contribution of higher periodicities, produced by the 4.5 μm sub-field of the e-beam writer. (b) This fades out when the sample is tempered. (c) The at-wavelengths efficiency of the gratings after annealing shows that tempering influences the processed grating and impacts the efficiency. (d) Profile of each of the gratings before etching is shown for illustrative purposes.

08 December 2025 09:12:47

© Author(s) 2025

At-wavelength measurements of the etched samples show how lower roughness values obtained by tempering decrease the contribution to the diffuse scattering [see Fig. 6(a)]. Although no difference is observed between the samples tempered at 115 or 120 °C in terms of diffuse scattering, the superperiodicity visible for the non-tempered sample, as well as for the lowest temperature, corresponds to the subfield of the e-beam writer of 4.5 μm [see Fig. 6(b)]. This contribution becomes negligible after increasing the annealing temperature. This effect can also be minimized by optimizing the writing process during e-beam writing, i.e., optimizing the direction and ordering of the exposures to minimize this impact. In terms of efficiency at the first diffraction order, lowering the facet roughness did not directly increase the grating efficiency [see Fig. 6(c)]. The negative influence that thermal annealing (at 120 °C during 120 min) has on the efficiency is attributed to the loss of sharpness in the apex region and the variation of the antiblaze-to-blaze ratio following annealing, as it was predicted in Fig. 2. Lines from the AFM measurements after tempering are shown in Fig. 6(d) to better illustrate the impact that tempering has on the overall shape as well as on the facet roughness of the grating. When changing the blaze angle, the maxima of efficiency are shifted on the energy axis. This is the case for the low diffraction order efficiency of the non-tempered sample in Fig. 6(a). For this reason, this sample was left out of the efficiency comparison. The corresponding quantitative values of roughness and the antiblaze-to-blaze ratio after etching are listed in Table II. The antiblaze-to-blaze angles are rather conserved, while roughness decreases (as well as the absolute value of the angles).

To achieve a grating with a specific blaze angle, the reshaping after tempering must be accounted for in the fabrication process. In a further analysis, the writing method was adapted to leave the apex region without being exposed, as it was previously tested by Schleunitz and Schift.[21] Figures 7(a) and 7(b) show the comparison of the fields before and after tempering. By only leaving one spot (1%) of the apex region without a dose [Fig. 7(a)], the desired effect was not totally achieved. It was observed that in order to be significant for a 600 lines/mm grating, at least 5% of the area at each period should not be exposed to any dose. This might be critical for very small periods, where the number of beam steps is reduced. This adjustment in the exposure resulted in improved antiblaze-to-blaze angular ratios (see Table III). Samples 4–7 were tempered using the same temperature but for different times. The samples indicated with * correspond to the ones where the exposure left out the apex regions of the grating. By doing that, the apex region remains sharp and pattern fidelity increases. However, also larger temperatures are allowed while reducing the tempering time.

TABLE III. AFM analysis of 600 lines/mm gratings in PMMA before (rms_i) and after (rms_t) thermal treatment at various durations.

Sample	rms_i (nm)	T (°C)	t (min)	rms_t (nm)	Antiblaze to blaze
4	1.1	125	15	0.6	5.6 ± 0.5
5[a]	1.1	125	15	0.6	6.6 ± 0.4
6	1.7	125	30	0.5	5.9 ± 0.4
7[a]	1.7	125	30	0.5	8.0 ± 0.5

[a]These samples were produced by adapting the exposure, allowing the apex region to not receive any dose; in this case, 5% of the total area of the facet was left out of the exposure. The impact of the adapted exposure can be seen in the AFM profiles, Fig. 7.

This redefined writing process was tested for higher line densities, where the beam steps are reduced. The same procedure was tested for one grating of 2400 lines/mm as well as for the extreme case of a grating with 290 nm periodicity (3448 lines/mm). In this latter case, the 5% of the total doses to expose a period corresponds to a unique shot. Figure 7(c) shows the AFM measurement for both gratings. For the extreme case, the antiblaze-to-blaze ratio is around 2.5. The case of 2400 lines/mm gratings shows a better angular ratio. In these cases, other approaches might be tested, such as leaving out

08 December 2025 09:12:47

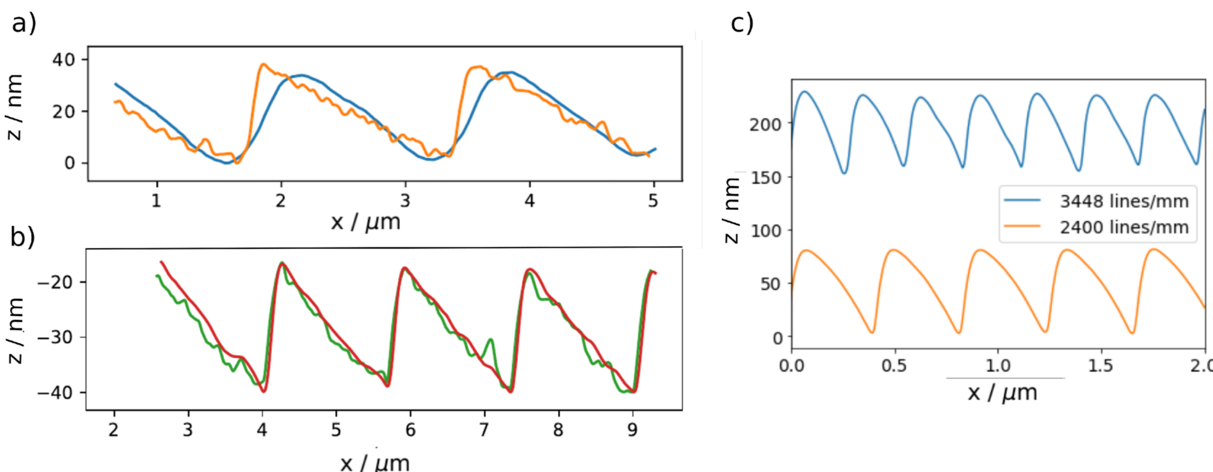

FIG. 7. AFM profiles of the gratings on PMMA. (a) Grating after tempering at 120 °C, following the procedure shown in Fig. 4(b). (b) and (c) Gratings produced using the adapted writing procedure described in Fig. 4(c), followed by tempering at 125 °C for 15 min. (c) shows high line density tests using the shape primitive *path* for e-beam dose control. These tests explore the limits of the adapted exposure method.

© Author(s) 2025

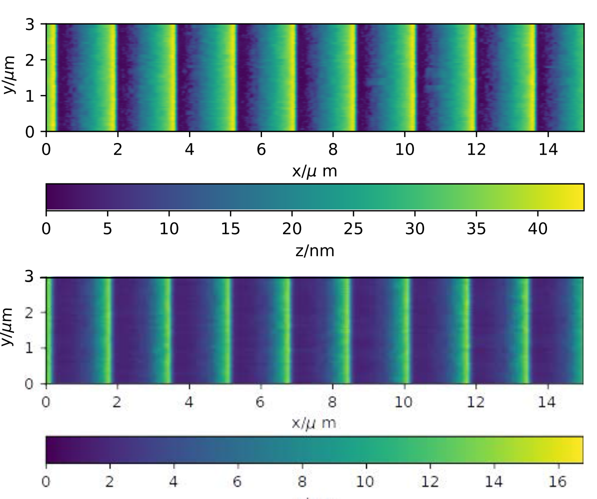

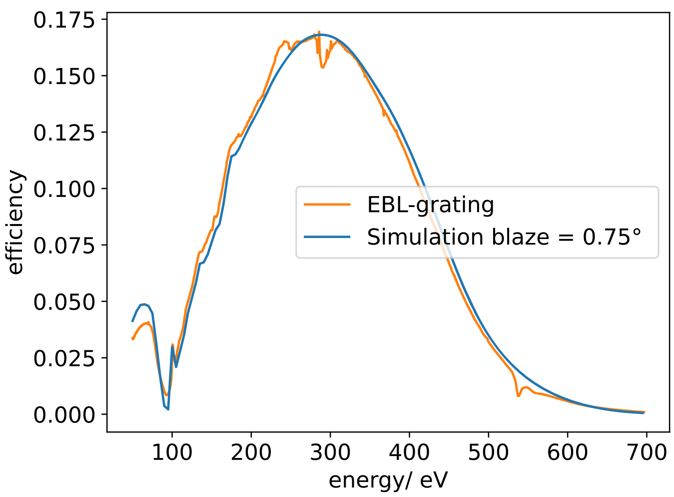

FIG. 8. AFM measurements of the grating before etching (top) and after etching (bottom). The facet roughness was 0.74 and 0.39 nm, respectively. On the right is the measured efficiency (orange) at-wavelengths of the etched blazed grating. The measured efficiency is compared to the simulation (blue) using REFLEC of an ideal blazed profile with a blaze angle of 0.75°.

of exposure a larger region at the apex, changing the overall parameters of the exposure, such as BSS, or varying the dose density by using multipass and gaining more flexibility.

Finally, a grating was produced following the aforementioned steps, a grating of 600 lines/mm with 0.75°. Figure 8 shows the AFM profile as well as the efficiency curve of such a grating. See Fig. 4(c) for a summary of the steps. By doing so, the roughness of the facet after etching in Si is 0.39 nm, and the antiblaze-to-blaze ratio is 6.5 ± 0.5. The expected efficiency was calculated using REFLEC for a grating with a blaze angle of 0.75° and an ideal antiblaze angle. The calculation and the measurement show a very good agreement, and the variations might be due to small variations of the grating profile. The AFM measurement, although performed at several locations, is still a local method, while the at-wavelength measurements give a global picture of how this type of grating would perform under real illumination. The simulated ideal profile does not consider any contamination from carbon or oxygen, as the measured efficiency of the grating does. Usually, this grating is used after coating it with a high-reflective material or a multilayer, depending on the energy region, and increasing its final efficiency.

Finally, a new shape primitive implemented by RAITH, named the *gradient cube*, was tested as well. It allows the variation of the dose along a defined axis. By corresponding this axis with the grating period, it is possible to create a grating with a specific blazed profile angle. This is achieved by adjusting the bottom and top doses of each facet, as determined by the contrast curve, and in between the dose is varied for each shot on the facet. This is similar to the procedure of using *path*, and so were the results. However, *gradient CUBE* simplified the process of writing blazed profile gratings using e-beam exposure and reduced the size of the created file, thus improving its readability and integration. This is crucial for more sophisticated e-beam exposures, such as those needed for variable line space gratings over large aperture areas.

IV. CONCLUSION

In this study, we show the feasibility of producing highly precise blazed gratings by means of EBL. Moreover, we show that the availability of dedicated metrology is a key factor in decision making in nanopatterning technology. The steps introduced in the process, such as tempering and a controlled exposure of the apex region, leverage the impact of the roughness on the facet as well as improve the overall shape of the blazed profile gratings. We find that by leaving 5% of the grating, corresponding to the apex region of the grating, unexposed, higher ratios of antiblaze to blaze angles can be obtained. However, this is challenged by very small gratings.

The patterning time of the EBL system for a 600 lines/mm grating would take a similar amount of time as mechanical ruling, considering as well the equilibration time inside the EB writer. However, the EBL writing time does not increase significantly with the line density, as is the case with mechanical ruling. The latter is a major advantage when producing large patterned apertures of significantly higher line density. In addition, EBL is very versatile, allowing us to control the resist exposure and adapt it locally, which makes this method perfectly suitable for the production of variable line space (VLS) gratings.

Follow-up studies on benchmarking EBL to other existing lithography methods can finally help to establish EBL as a patterning technology for blazed profile gratings in small and medium sized apertures. Upcoming work should also cover investigations on modifying the concept of reflection zone plates (RZPs)[37,38] toward RZPs with a blazed groove profile instead of laminar. However, the

08 December 2025 09:12:47

© Author(s) 2025

thermal load on the substrates of these optical elements in FELs and synchrotron radiation facilities is still a topic to be addressed.

ACKNOWLEDGMENTS

This research was supported by the European Union's Horizon 2020 research and innovation program under Grant Agreement No. 101004728 (LEAPS-INNOV). The authors would like to acknowledge all our partners within the LEAPS-INNOV WP4-NeXtgrating cooperation for their very useful discussions and exchange of ideas. A.F.H., A.S., and F.S. are very grateful to Alexei Erko (formerly at HZB) for many years of co-working, sharing his ideas with us, and for profound discussions on the topics shown in this publication.

AUTHOR DECLARATIONS

Conflict of Interest

The authors have no conflicts to disclose.

Author Contributions

Analía F. Herrero: Conceptualization (equal); Formal analysis (lead); Investigation (lead); Methodology (lead); Project administration (equal); Software (equal); Validation (equal); Visualization (lead); Writing – original draft (lead); Writing – review & editing (lead). **Nazanin Samadi**: Conceptualization (equal); Formal analysis (supporting); Investigation (equal); Methodology (supporting); Project administration (equal); Software (supporting); Writing – review & editing (supporting). **Andrey Sokolov**: Formal analysis (supporting); Investigation (equal); Resources (equal). **Grzegorz Gwalt**: Data curation (supporting); Investigation (supporting); Methodology (supporting); Software (supporting). **Stefan Rehbein**: Conceptualization (equal); Investigation (supporting); Methodology (equal); Resources (equal); Supervision (equal); Writing – review & editing (equal). **Anke Teichert**: Investigation (supporting). **Bas Ketelaars**: Methodology (supporting); Software (equal). **Christiaan Zonnevylle**: Funding acquisition (supporting); Methodology (supporting); Resources (equal); Software (supporting). **Thomas Krist**: Funding acquisition (supporting); Resources (equal). **Christian David**: Conceptualization (equal); Funding acquisition (lead); Project administration (lead); Validation (equal); Writing – review & editing (equal). **Frank Siewert**: Conceptualization (equal); Funding acquisition (lead); Project administration (lead); Resources (equal); Validation (equal); Writing – original draft (supporting); Writing – review & editing (equal).

DATA AVAILABILITY

The data that support the findings of this study are available from the corresponding author upon reasonable request.

REFERENCES

[1]M. Eriksson, J. F. van der Veen, and C. Quitmann, "Diffraction-limited storage rings—A window to the science of tomorrow," J. Synchrotron Radiat. **21**, 837 (2014).

[2]J. H. Underwood, C. K. Malek, E. M. Gullikson, and M. Krumrey, "Multilayer-coated echelle gratings for soft x rays and extreme ultraviolet," Rev. Sci. Instrum. **66**, 2147–2150 (1995).

[3]H. Lin, L. Zhang, L. Li, C. Jin, H. Zhou, and T. Huo, "High-efficiency multilayer-coated ion-beam-etched blazed grating in the extreme-ultraviolet wavelength region," Opt. Lett. **33**, 485–487 (2008).

[4]D. Cocco, G. Cutler, M. Sanchez del Rio, L. Rebuffi, X. Shi, and K. Yamauchi, "Wavefront preserving x-ray optics for synchrotron and free electron laser photon beam transport systems," Phys. Rep. **974**, 1–40 (2022).

[5]J. Gaudin, C. Ozkan, J. Chalupský, S. Bajt, T. Burian, L. Vyšín, N. Coppola, S. D. Farahani, H. N. Chapman, G. Galasso, V. Hájková, M. Harmand, L. Juha, M. Jurek, R. A. Loch, S. Möller, M. Nagasono, M. Störmer, H. Sinn, K. Saksl, R. Sobierajski, J. Schulz, P. Sovak, S. Toleikis, K. Tiedtke, T. Tschentscher, and J. Krzywinski, "Investigating the interaction of x-ray free electron laser radiation with grating structure," Opt. Lett. **37**, 3033–3035 (2012).

[6]J. Krzywinski, R. Conley, S. Moeller, G. Gwalt, F. Siewert, C. Waberski, T. Zeschke, and D. Cocco, "Damage thresholds for blaze diffraction gratings and grazing incidence optics at an X-ray free-electron laser," J. Synchrotron Radiat. **25**, 85–90 (2018).

[7]A. Sokolov, Q. Huang, F. Senf, J. Feng, S. Lemke, S. Alimov, J. Knedel, T. Zeschke, O. Kutz, T. Seliger, G. Gwalt, F. Schäfers, F. Siewert, I. V. Kozhevnikov, R. Qi, Z. Zhang, W. Li, and Z. Wang, "Optimized highly efficient multilayer-coated blazed gratings for the tender X-ray region," Opt. Express **27**, 16833–16846 (2019).

[8]S. Werner, P. Guttmann, F. Siewert, A. Sokolov, M. Mast, Q. Huang, Y. Feng, T. Li, F. Senf, R. Follath, Z. Liao, K. Kutukova, J. Zhang, X. Feng, Z.-S. Wang, E. Zschech, and G. Schneider, "Spectromicroscopy of nanoscale materials in the tender X-ray regime enabled by a high efficient multilayer-based grating monochromator," Small Methods **7**, 2201382 (2023).

[9]S. Wen, Q. Huang, A. Sokolov, Y. Zhuang, S. Lemke, T. Seliger, Y. Yu, J. Viefhaus, R. Qi, Z. Zhang, and Z. Wang, "High efficiency multilayer coated laminar gratings with high line density for tender X-ray region," Opt. Laser. Technol. **168**, 109979 (2024).

[10]Q. Huang, I. V. Kozhevnikov, A. Sokolov, Y. Zhuang, T. Li, J. Feng, F. Siewert, J. Viefhaus, Z. Zhang, and Z. Wang, "Theoretical analysis and optimization of highly efficient multilayer-coated blazed gratings with high fix-focus constant for the tender X-ray region," Opt. Express **28**, 821–845 (2020).

[11]F. Siewert, B. Löchel, J. Buchheim, F. Eggenstein, A. Firsov, G. Gwalt, O. Kutz, S. Lemke, B. Nelles, I. Rudolph, F. Schäfers, T. Seliger, F. Senf, A. Sokolov, C. Waberski, J. Wolf, T. Zeschke, I. Zizak, R. Follath, T. Arnold, F. Frost, F. Pietag, and A. Erko, "Gratings for synchrotron and FEL beamlines: A project for the manufacture of ultra-precise gratings at Helmholtz Zentrum Berlin," J. Synchrotron Radiat. **25**, 91–99 (2018).

[12]S. Dziarzhytski, F. Siewert, A. Sokolov, G. Gwalt, T. Seliger, M. Rübhausen, H. Weigelt, and G. Brenner, "Diffraction gratings metrology and ray-tracing results for an XUV Raman spectrometer at FLASH," J. Synchrotron Radiat. **25**, 138–144 (2018).

[13]D. L. Voronov, S. Park, E. M. Gullikson, F. Salmassi, and H. A. Padmore, "Advanced low blaze angle x-ray gratings via nanoimprint replication and plasma etch," Opt. Express **31**, 26724–26734 (2023).

[14]Y. Fujii, K. Aoyama, and J. Minowa, "Optical demultiplexer using a silicon echelette grating," IEEE J. Quantum Electron. **16**, 165–169 (1980).

[15]P. Philippe, S. Valette, O. M. Mendez, and D. Maystre, "Wavelength demultiplexer: Using echelette gratings on silicon substrate," Appl. Opt. **24**, 1006–1011 (1985).

[16]Q. Nie, Y. Xie, and F. Chang, "MEMS blazed gratings fabricated using anisotropic etching and oxidation sharpening," AIP Adv. **10**, 065216 (2020).

[17]S. Zha, D. Li, Q. Wen, Y. Zhou, and H. Zhang, "Design and fabrication of silicon-blazed gratings for near-infrared scanning grating micromirror," Micromachines **13**, 1000 (2022).

[18]D. L. Voronov, S. Park, E. M. Gullikson, F. Salmassi, and H. A. Padmore, "6000 lines/mm blazed grating for a high-resolution x-ray spectrometer," Opt. Express **30**, 28783–28794 (2022).

[19]W. Henke, W. Hoppe, H. Quenzer, P. Staudt-Fischbach, and B. Wagner, "Simulation and experimental study of gray-tone lithography for the fabrication of arbitrarily shaped surfaces," in *Proceedings IEEE Micro electro Mechanical Systems*

08 December 2025 09:12:47

© Author(s) 2025

an Investigation of Micro Structures, Sensors, Actuators, Machines and Robotic Systems (IEEE, 1994), pp. 205–210.
[20] Z. Shi, K. Jefimovs, L. Romano, and M. Stampanoni, "Towards the fabrication of high-aspect-ratio silicon gratings by deep reactive ion etching," Micromachines **11**, 864 (2020).
[21] A. Schleunitz and H. Schift, "Fabrication of 3D nanoimprint stamps with continuous reliefs using dose-modulated electron beam lithography and thermal reflow," J. Micromech. Microeng. **20**, 095002 (2010).
[22] J. A. McCoy, R. L. McEntaffer, and C. M. Eichfeld, "Fabrication of astronomical x-ray reflection gratings using thermally activated selective topography equilibration," J. Vac. Sci. Technol., B: Nanotechnol. Microelectron.: Mater., Process., Meas., Phenom. **36**, 06JA01 (2018).
[23] T. B. Borzenko, Y. I. Koval, and V. A. Kudryashov, "Ion beam etching mechanism of PMMA based resists by noble gas ions," Microelectron. Eng. **23**, 337–340 (1994).
[24] V. Guzenko and C. David, "Fabrication of blazed diffractive optics by through-mask oxidation," U.S. patent 2019P20969WO (2019).
[25] A. Schleunitz, V. A. Guzenko, A. Schander, M. Vogler, and H. Schift, "Selective profile transformation of electron-beam exposed multilevel resist structures based on a molecular weight dependent thermal reflow," J. Vac. Sci. Technol., B: Nanotechnol. Microelectron.: Mater., Process., Meas., Phenom. **29**, 06F302 (2011).
[26] J. A. McCoy, R. L. McEntaffer, and D. M. Miles, "Extreme ultraviolet and soft X-ray diffraction efficiency of a blazed reflection grating fabricated by thermally activated selective topography equilibration," Astrophys. J. **891**, 114 (2020).
[27] R. C. McCurdy, D. M. Miles, J. A. McCoy, F. Grisé, and R. L. McEntaffer, "Diffraction efficiency of a small-period astronomical x-ray reflection grating fabricated using thermally activated selective topography equilibration," J. Astron. Telesc. Instrum. Syst. **6**, 045003 (2020).
[28] A. Schleunitz, V. A. Guzenko, M. Messerschmidt, H. Atasoy, R. Kirchner, and H. Schift, "Novel 3D micro- and nanofabrication method using thermally activated selective topography equilibration (taste) of polymers," Nano Convergence **1**, 7 (2014).
[29] S. Lemke, S. Alimov, J. Knedel, O. Kutz, I. Rudolph, T. Seliger, and A. Sokolov, "Low line density blazed gratings with low blaze angles," J. Phys.: Conf. Ser. **2380**, 012057 (2022).
[30] R. Follath, J. S. Schmidt, M. Weigand, K. Fauth *et al.*, "The X-ray microscopy beamline UE46-PGM2 at BESSY," AIP Conf. Proc. **1234**, 323–326 (2010).
[31] F. Schäfers, P. Bischoff, F. Eggenstein, A. Erko, A. Gaupp, S. Künstner, M. Mast, J.-S. Schmidt, F. Senf, F. Siewert, A. Sokolov, and T. Zeschke, "The at-wavelength metrology facility for UV- and XUV-reflection and diffraction optics at BESSY-II," J. Synchrotron Radiat. **23**, 67–77 (2016).
[32] D. E. Starr, M. Hävecker, A. Knop-Gericke, M. Favaro, S. Vadilonga, M. Mertin, G. Reichardt, J.-S. Schmidt, F. Siewert, R. Schulz, J. Viefhaus, C. Jung, and R. van de Krol, "The Berlin joint lab for electrochemical interfaces, BElChem: A facility for *in-situ* and operando NAP-XPS and NAP-HAXPES studies of electrochemical interfaces at BESSY II," Synchrotron Radiat. News **35**, 54–60 (2022).
[33] T. Mortelmans, D. Kazazis, V. A. Guzenko, C. Padeste, T. Braun, H. Stahlberg, X. Li, and Y. Ekinci, "Grayscale e-beam lithography: Effects of a delayed development for well-controlled 3D patterning," Microelectron. Eng. **225**, 111272 (2020).
[34] D. Nečas and P. Klapetek, "Gwyddion: An open-source software for SPM data analysis," Open Phys. **10**, 181–188 (2012).
[35] D. Nečas, M. Valtr, and P. Klapetek, "How levelling and scan line corrections ruin roughness measurement and how to prevent it," Sci. Rep. **10**, 15294 (2020).
[36] A. Sokolov, M. G. Sertsu, A. Gaupp, M. Lüttecke, and F. Schäfers, "Efficient high-order suppression system for a metrology beamline," J. Synchrotron Radiat. **25**, 100–107 (2018).
[37] A. Erko, A. Firsov, R. Gubzhokov, A. Bjeoumikhov, A. Günther, N. Langhoff, M. Bretschneider, Y. Höhn, and R. Wedell, "New parallel wavelength-dispersive spectrometer based on scanning electron microscope," Opt. Express **22**, 16897–16902 (2014).
[38] C. Braig, H. Löchel, R. Mitzner, W. Quevedo, P. Loukas, M. Kubin, C. Weniger, A. Firsov, J. Rehanek, M. Brzhezinskaya, P. Wernet, A. Föhlisch, and A. Erko, "Design and optimization of a parallel spectrometer for ultra-fast X-ray science," Opt. Express **22**, 12583–12602 (2014).

08 December 2025 09:12:47

© Author(s) 2025